A Superhydrophobic Coating : Fluorophilic Silica Nanoparticle-Doped Teflon Films

by

Sijia Wang

BS, Shandong University, 2010

Submitted to the Graduate Faculty of

The Kenneth P. Dietrich School of

Arts and Sciences in partial fulfillment

of the requirements for the degree of

Master of Science

UNIVERSITY OF PITTSBURGH

2013

UNIVERSITY OF PITTSBURGH

DIETRICH SCHOOL OF ARTS AND SCIENCES

This thesis was presented

by

Sijia Wang

It was defended on

August 9, 2013

and approved by

Dr. Haitao Liu, Assistant Professor, Department of Chemistry

Dr. Jill Millstone, Assistant Professor, Department of Chemistry

Thesis Director: Dr. Stephen G. Weber, Professor, Department of Chemistry

Prof. Stephen G. Weber

A Superhydrophobic Coating : Fluorophilic Silica Nanoparticle Doped Teflon Films

Sijia Wang, MS

University of Pittsburgh, 2013

Coatings prepared from a suspension of fluoroalkyl-silane modified silica nanoparticles (FNPs) in a solution containing Teflon AF 2400 show wetting properties that depend on composition and the method of film formation. Static contact angle and sliding angle measurements revealed that adding FNPs improved their water repellency. Specifically, water droplets have static contact angles of 120-151 ° on FNP-containing films, compared with 114.6° on a FNP-free Teflon AF coated surface. Static contact angles increase with the weight percent of FNPs. Superhydrophobic (contact angle >150° and sliding angle <10°) states were achieved on films with 70% weight percentage of 510 nm FNPs. Surface morphologies were determined by scanning electron microscopy (SEM) and atomic force microscopy (AFM). Spin coating was later proved a better film fabrication method than solution-cast deposition, in terms of surface morphology and sliding angles.

TABLE OF CONTENTS

1.0 INTRODUCTION 1

1.1 SUPERHYDROPHOBIC SURFACE 1

1.2 MODELS OF SUPERHYDROPHOBIC STATES 2

1.3 FLUOROUS MATERIALS: TEFLON AF 2400 3

2.0 EXPERIMENTAL SECTION 8

2.1 REAGENTS 8

2.2 NANOPARTICLE PREPARATION AND FLUORINATION 8

2.3 FILM PREPARATION AND CHARACTERIZATION 10

3.0 RESULTS AND DISCUSSION 12

3.1 PROPERTIES OF FLUOROUS SILICA PARTICLES 12

3.1.1 Preparation of Silica Particles 12

3.1.2 Characterization of Silica Particles 13

3.2 WETTING PROPERTIES 14

3.3 SURFACE MORPHOLOGY ANALYSIS 18

3.4 SOLUTION-CAST DEPOSITION 21

4.0 CONCLUSION 25

ACKNOWLEDGEMENT 26

BIBLIOGRAPHY 27

LIST OF TABLES

Table 1. Summary of wettability measurements and comparasion to calculated values..... 20

LIST OF FIGURES

Figure 1. Wetting state (a) Wenzel, (b) Cassie –Baxter and (c) combined models 3

Figure 2. Three immiscible phases 4

Figure 3. Structure of Teflon AF 2400 5

Figure 4. Dependece of partice size on initial ammonium concentration..... 12

Figure 5. SEM images of particles with 50, 120, 300 and 510 nm diameter..... 13

Figure 6. Static contact angle measurement on Teflon AF 2400 films with 5%, 10%, 15%, 30%, 50%, 70% and 85% (wt%) 510 nm FNP 16

Figure 7. Static contact angle (a) and sliding angle (b) of 4 µL water on spin-coat surfaces. Films were prepared with 120, 310 and 510 nm FNPs, with wt% of 5%, 10%, 15%, 30%, 50%, 70% and 85% 17

Figure 8. AFM images of (a) 120 nm, (b) 310 nm and (c) 510 nm FNP (wt% = 70%) doped Teflon films with 5 µm scan size..... 18

Figure 9. Static contact angle and sliding angle of spin coat and solution – cast 120 nm FNP doped Teflon films..... 23

Figure 10. SEM images and of (a) spin-coat and (b) solution-cast deposited films with 70% (wt%) 120nm FNP 24

1.0 INTRODUCTION

1.1 SUPERHYDROPHOBIC SURFACE

Surfaces with a water contact angle greater than 150° and a sliding angle less than 10° are defined as superhydrophobic[1-3]. It was discovered that some natural surfaces, such as the lotus leaf[4,5], exhibit remarkable water-repellent and self-cleaning properties[6] based on their combination of a hydrophobic wax layer and a hierarchically rough microstructure. Recently, fabricated superhydrophobic surfaces have found their applications in areas such as dust-free coatings, water-proof textiles, and microfluidic devices[7].

As described by Cassie and Baxter[8], multi-level roughness enables trapping of air under the water droplet, enhancing the surface hydrophobicity[8-11]. Microstructured pillar arrays fabricated by photolithography[12,13] and soft lithography[14,15] are often used to provide a predefined roughness. The major issues facing wide application of these techniques include high fabrication cost, limited application to large scale coating, and reduced flexibility in modulation of surface morphologies. One of the low-cost alternatives is through surface deposition of nanoparticles[16-19]. As silica nanoparticles are readily synthesized by a sol-gel process[20-22] with uniform size, and as their surface chemistry is tunable via covalent modification, they are widely used in creating surfaces with desirable properties. Tsai et al. have fabricated raspberry-like particulate coatings by layer-by-layer assembly of two different sizes of silica nanoparticles,

which resulted in superhydrophobic surfaces[23]. Karunakaran et al. reported on superhydrophobic film prepared by sequential dip coating of 3-aminopropyltrimethoxysilane-functionalzied silica particles of two different sizes (20 and 100 nm)[24]. Ling et al. have created stable and transparent superhydrophobic films by deposition of silica nanoparticles onto an amine-terminated substrate, followed by 1*H*, 1*H*, 2*H*, 2*H*-perfluorodecyltriethoxysilane (PFTS) gas-phase deposition[25]. Ogihara et al. recently reported on spraying alkylsilane-modified nanoparticles on paper substrates[26]. Moreover, randomly packed surfaces prepared via spin coating usually have enhanced surface roughness than the hexagonally ordered structures[27].

1.2 MODELS OF SUPERHYDROPHOBIC STATES

Wenzel's[28] and Cassie and Baxter's[8] models are used to explain the effect of surface roughness on its wettability (Fig 1). According to Wenzel, liquid is in intimate contact with the structured surface, and hydrophobicity is due to the enhanced surface area of solid. The contact angle derived from this model is given as:

$$\cos\Theta_e^{W} = r\cos\Theta_o$$

where the roughness factor $r > 1$is the ratio of the true surface area and the projected area, and Θ_o is the contact angle on flat surface. Wenzel's model applies only when the flat surfaces is hydrophobic (Θ_o>90°), otherwise adding roughness will make the surface more hydrophilic.

In the Cassie-Baxter model, water does not completely penetrate into the spaces on the surface, and air remains trapped under the water drop. Consequently, the droplet sits partially on

the solid with *f* as the fraction of the surface area that contacts the droplet, and (1- *f*) as the fraction of the droplet in contact with trapped air. The contact angle is

$$\cos\Theta^{C\text{-}B} = f(\cos\Theta_o + 1) - 1.$$

This model is frequently applied to surfaces with small sliding angle, which is defined as a critical angle where a water drop begins to roll off the tilted surface. Surfaces with complex roughness can be described in terms of both models[29-31].

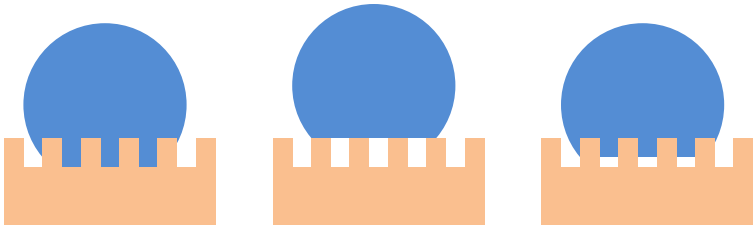

(a) (b) (c)

Fig. 1 Wetting states (a) Wenzel, (b) Cassie-Baxter, and (c) combined models

1.3 FLUOROUS MATERIALS: TEFLON AF 2400

Fluorous compounds are defined as "*of, relating to, or having the characteristics of highly fluorinated saturated organic materials, molecules, or molecular fragments*"[32]. Fluorocarbons generally form a separate phase in the presence of organic solvent and water (Fig. 2). This unusual miscibility property is due to the large difference of the Hildebrand's solubility parameter[33], δ, which is defined as the square root of the cohesive energy density, or the heat needed for vaporization of a pure component over its molar volume. For example, the difference in solubility parameter makes perfluorohexane (δ_f = 12.3 $MPa^{1/2}$) phase separate from hexane

(δ_o = 14.9 $MPa^{1/2}$)[33]. The decreased solubility parameters for fluorocarbons are due to the weak van der Waals interactions between the F-containing compounds. Therefore, fluorocarbons are expected to partition to fluorous over organic or aqueous solvent. This tendency is termed "fluorophilic"[34].

Fig.2 Three immiscible phases

Organic solutes are rendered "fluorophilic" by covalently functionalizing them with one or more fluorocarbon ponytails $[(CH_2)_m(CF_2)_{n-1}CF_3]$[35].Thus modified, organic compounds become more compatible with fluorous solvents. Generally, solubility depends on the length and composition of the fluorocarbon chains. More incorporated $-CF_2-$ groups results in a smaller solubility parameter and a larger partition coefficient to fluorous solvents. Moreover, the partition coefficients of fluorous solutes in fluorous biphasic systems can be estimated based on the structure of solutes[36]. The reduced solubility parameter improves the transport selectivity of fluorous solvents for fluorinated molecules over non-fluorous compounds, and consequently benefits its application in preparation of selective extraction devices, biphasic catalytic recycling system, as well as hydrophobic surfaces[37-41].

Generally, the wettability behavior of rough surfaces is governed by the interface chemistry. Specifically, hydrophobicity is favored with reduced surface energy[42], which inspires the use of fluoroalkyl $[(CH_2)_m(CF_2)_{n-1}CF_3]$ functionalized materials and perfluoropolymers[12,43-47].

For example, Raza et al. applied 1*H*, 1*H*, 2*H*, 2*H*-perfluorodecyltichlorosilane to control the wetting behavior of silica nanoparticle arrays[48]. Lau et al. used a poly(tetrafluoroethylene) (surface energy 18 mN/m) coating to reduce the adhesion in vertically aligned carbon nanotube forests[49]. Recently, Brassard et al. reported on layer-by-layer thin film coatings prepared using fluorinated silica nanoparticles only[46,50]. However, such coatings were fragile considering their all-particle composition. Nilsson et al. fabricated surfaces with hydrophobic properties on Teflon by roughing the surface with sandpaper[51]. Recently, Singh et al. reported on Teflon coated graphene sheet as a stable superhydrophobic structure[52]. However, the influence of graphene structure on its wetting behavior was not fully discussed. And also, the template-directed vapor deposition method they used can be expensive and laborious.

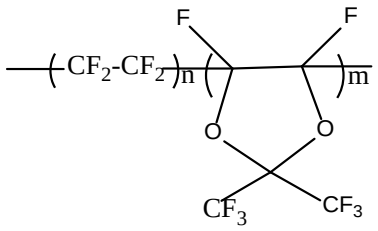

Teflon AF 2400

Fig. 3 The structure of Teflon AF 2400

Herein Teflon AF 2400 was employed in fabricating superhydrophobic films. As a commercially available, soluble perfluoropolymer, Teflon AF 2400 (Fig. 3) is widely used to take advantage of its solubility, thermal and chemical stability, mechanical robustness, as well as the low surface energy (~16 mN/m)[53]. For instance, Teflon AF has been used to coat a wide variety of roughened surfaces, e.g., aluminum[54,55], ZnO[56], steel with an electropolymerized layer[57], and fiber mats of carbon[58] and glass[59]. While these approaches are very useful, their

wettability depends upon the underlying material structure. Electrospun fibers with Teflon AF have been created[60-62]. These fibers can be used as a coating to form superhydrophobic surfaces from, in principle, any material. Liu et al. have created an approach in which alkyl or fluoroalkyl-containing particles created in a sol-gel process are combined with a latex formulation and a crosslinker[63,64]. This mixture can be sprayed onto, for example, fabrics to create effectively superhydrophobic materials. Formulations for superhydrophobic coatings that do not depend on the inherent roughness of the substrate, and which do not require complex processing are desirable.

Despite the wide use of Teflon AF and nanoparticles in superhydrophobic studies, combinations of the two are surprisingly rare. Bayer et al. fabricated hydrophobic coatings on sandpapers on which submicrometer Teflon particles (average size of ~150 nm) were deposited[65]. This work has limitations, however, as the surface roughness was largely dependent on the substrate morphology and the sliding angles are as high as ~10 ° to ~ 40 °. Liu et al. in one of their formulations used a latex incorporating a fluoropolymer with hydroxyl groups. In the process of deposition by spin coating, the sol-gel process creates silica particles (μm dimensions) with a bumpy, strawberry-like surface of fluorpolymer latex particles[63].

Our desire was to understand a simple system containing fluorous nanoparticles and a fluoropolymer binder. Our goal was to find the dependence of contact angle and sliding angle on particle size and composition. In our work, Teflon AF films were created by both spin-coating and casting (slow solvent evaporation) on smooth glass slides. The effect of the presence of FNPs was evaluated quantitatively. Suspensions of Teflon AF 2400 and FNPs with different diameters with various weight percent FNPs were used in the coating process. The dependence of surface wettability on the particle sizes and the weight percent of FNPs (wt% $_{FNP}$) were

investigated. Spin coating[66] was compared with solution-cast deposition[67,68] for one particle diameter.

2.0 EXPERIMENTAL SECTION

2.1 REAGENTS

Colloidal silica particle with 120 nm diameter (IPA-ST-ZL) was a gift from Nissan Chemical Co. (Tokyo, Japan). Telflon AF 2400 was purchased from DuPont (Wilmington, DE). HFE-7100 (a mixture of methyl nonafluorobutyl and nonafluoroisobutyl ethers) and Fluorinert FC-72 (a mixture of perfluorohexanes) were purchased from 3M (Minneapolis, MN). 1*H*, 1*H*, 2*H*, 2*H*-perfluorooctyltriethoxysilane, ammonium hydroxide (28%-30%), tetraethylorthosilicate (TEOS), ethanol and isopropanol were obtained from Sigma-Aldrich (St. Louis, MN).

2.2 NANOPARTICLE PREPARATION AND FLUORINATION

In a typical sol-gel process, the concentration of ammonium hydroxide is a strong factor in determining the final size of the silica particles[21]. Accordingly, a series of pilot experiments were conducted to determine this dependence. In a 500 mL flask, 5.6 mL TEOS was stirred with 19.4 mL ethanol. Following a short time, 18 mL of ethanol and 6 mL H_2O were added. After stirring for 10 minutes, a certain amount of ammonium hydroxide (0.5, 1.0, 1.5 and 2.0 mL, respectively) was added. To avoid a sharp increase in local concentration, which usually result in

discrepancy in particle size, it was added with syringe with a rate controlled at 5 seconds per drop. Particle diameters were measured after 2, 4 and 10 hours with dynamic light scattering.

Large particles, 510 and 310 nm, were synthesized as follows. To prepare the 510 nm silica particles, the staring materials, namely TEOS, H_2O, and ethanol were added exactly as in the pilot trials, and the hydrolysis step was allowed to proceed for 10 minutes. Following this, a solution of 2 mL ammonium hydroxide was added with syringe and the reaction was allowed to proceed at room temperature for 5 hours. The suspension was centrifuged at 6000 rpm for 30 minutes. The pellet was resuspended in fresh ethanol to wash away unreacted TEOS. To obtain 310 nm silica particles, a solution of 120 nm silica (IPA-ST-ZL, 2 mL) was stirred with 27 mL isopropanol at room temperature, followed by adding 15 mL TEOS. Then a mixture of 1.5 mL ammonium hydroxide in a solution of 20 mL isopropanol and 6 mL H_2O was added as catalyst. The reaction proceeded for 5 hours. The workup process was the same as above.

A typical procedure for particle modification included: 1) suspend silica nanoparticles (3.0 g) in a solution of isopropanol (35 mL) and HFE-7100 (25 mL); 2) add 1*H*, 1*H*, 2*H*, 2*H*-perfluorooctyltriethoxysilane (2 mL) as flouroalkane tags; and 3) add ammonium hydroxide (10 mL) in isopropanol (25 mL) to modulate the pH to about 10. The reaction mixture was then refluxed in an oil bath at 80 °C for 3 days. The modified nanoparticles was centrifuged (6000 rpm, 30 minutes) and resuspended in fresh washing solvent (ethanol: HFE-7100 = 2:1; v/v) for 3 cycles to wash away excess silane reagent.

For imaging, the suspension of silica particles in ethanol was spread on micro glass slides, and then sputter-coated with palladium to enhance surface conductivity. The images of silica particles were captured using a Philips XL-30 SEM (Hillsboro, OR).

2.3 FILM PREPARATION AND CHARACTERIZATION

Glass microscope slides (25 x 19 x 1 mm) from Fisher Scientific (Hampton, NH) were used as film casting substrates. To remove dust and impurities, the glass slides were cleaned with a heated mixture of concentrated sulfuric acid and hydrogen peroxide (piranha solution) at a ratio of 3:1 (v/v). (Caution: Piranha solution reacts violently with organic compounds and should be handled with extreme care.) This process was performed at 80 °C for 30 minutes, followed by rinsing with D.I. water. Cleaned glass slides were reserved in fresh ethanol.

To prepare the coating solution, FNPs (120, 310 and 510 nm) were mixed with Teflon AF 2400 in a solvent of FC-72 (2.5 mL) at room temperature to form a homogeneous suspension. In each solution, the total mass of FNP and Teflon AF 2400 was 62.5 mg, with $wt\%_{FNP}$ varying from 5% to 85%. Films were prepared by spin coating at 3000 rpm on the substrates layer by layer (4 layers in total) at a constant spin time of 40 seconds, before they were cured at 120 °C overnight.

FNP doped Teflon AF 2400 films were prepared by solution-cast deposition, as a comparison with the spin coating method. A total amount of 125 mg FNP and Teflon AF 2400 were mixed in 5 mL solvent of HFE-7100/ FC-77 = 2 : 1 (v/v), with $wt\%_{FNP}$ vary from 5% to 70%. In a casting process, the coating solution evaporates slowly in an optical-flat-bottomed Petri dish (i.d. 6.0 cm) at room temperature for 5-7 days until a solid film is formed. To get controlled evaporation, the dish was covered carefully to ensure an environment of saturated solvent vapor, and the casting platform was kept steady during the process.

The wetting properties were later characterized with a VCA 2000 video contact angle system (Advanced Surface Technology, Inc. Billerica, MA) with 4 μL droplets. Advancing and receding angles were measured by automatically adding/withdrawing water with a needle in the

water droplet. Contact angles were measured when water drop started to expand /contract. Sliding angles were calculated as the averaged difference in advancing and receding angle. All values were averaged over three different spots. Surface morphology was investigated with a Philips XL-30 SEM (Hillsboro, OR) after being sputter-coated with palladium. AFM measurements were conducted by PPG Industries (PA) with Digital Instruments Dimension 3000 microscope (Bruker Nano, Karlsruhe, Germany).

3.0 RESULTS AND DISCUSSION

3.1 PROPERTIES OF FLUOROUS SILICA PARTICLES

3.1.1 Preparation of Silica Particles

As shown in Fig. 4, the size of synthesized silica nanoparticles is affected by the initial concentration of ammonia. Particle size increases during the first 4 hours and then growth stops. Based on the result, 2 mL of ammonia were used in preparation of 510 nm silica particles and 1.5 mL was used for the 310 nm.

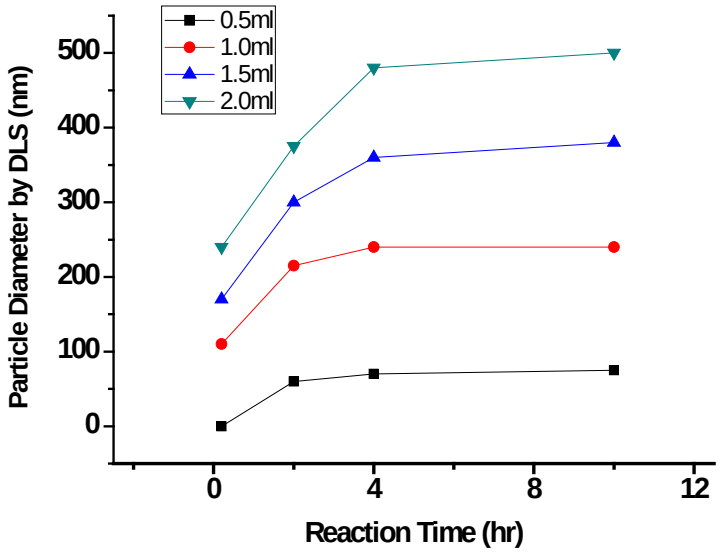

Fig. 4 Dependence of particle size on initial ammonia concentration.

3.1.2 Characterization of Silica Particles

Particle diameters were measured with SEM (Fig. 5). The 310 and 510nm particles show low polydispersity in SEM images, indicating the effectiveness of the sol-gel process in particle synthesis. Also notice that twin and triplet silica particles were found in the 310 nm preparation.

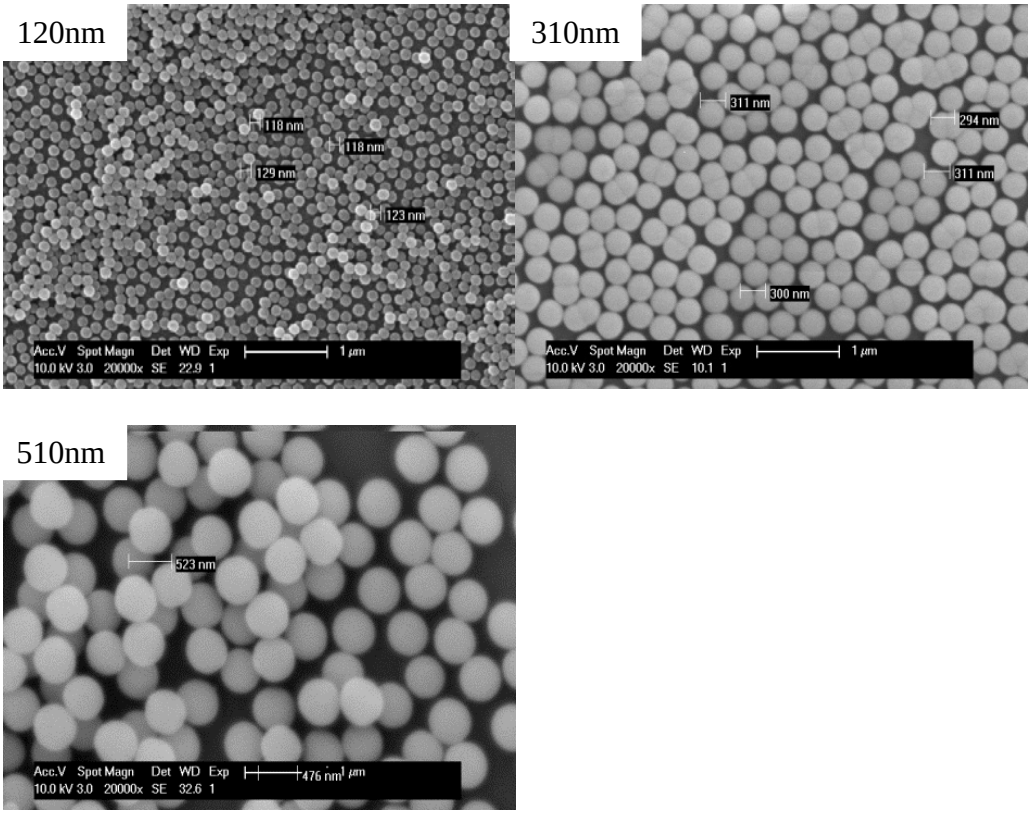

Fig.5 SEM images of particles with 120, 310 and 510 nm diameter

According to elemental analysis (C, H, F %), the surface concentrations of fluoroalkyl tags on 120, 310 and 510 nm FNPs are 3.2 ± 0.1, 7.2 ± 0.2 and 7.6 ± 0.1 μmol/m^2, respectively. These values are based on the assumption that the fluoroalkyl tags are the only source of fluorine, and that the specific surface areas are those of nonporous spheres, 30.0, 13.5 and 7.1 m^2/g for 120, 310 and 510 nm particles, respectively. The surface concentration of F-tag is

calculated via the following equation (atomic mass of fluorine is 19 g/mol and 13 fluorines per molecule):

$$surface\ concentration\ = \frac{\frac{F\ \%}{19*13}}{(1 - C\ \% - F\ \% - H\ \%) * specific\ surface\ area}$$

The surface coverages for the 310 and 510 nm particles are high as the surface coverage of silanol groups on silica particle is ~8 μmol/m^2. We infer that there is some porosity or roughness at the surface of the 310 and 510 nm particles.

3.2 WETTING PROPERTIES

Fig. 6 shows the static contact angles of films with particles of different diameters (120, 310 and 510 nm) and weight percentages (5%, 10%, 15%, 30%, 50%, 70% and 85%). As shown in Fig. 7 (a), the static contact angle generally increases with wt% $_{FNP}$. For the 510 nm FNP doped Teflon films, for instance, those with 5%, 10%, 15%, 30% and 50% FNPs have static contact angles of 126.2 ± 0.6, 126.6 ± 0.3, 137.8 ± 0.5 and 146 ± 0.4°, respectively. Stated errors are the standard deviation of the mean. Further increasing the FNP weight percentage to 85%, however, decreases the static contact angle to 148.4 ± 1.0°. This trend is also observed in 310 nm FNP doped Teflon films, where the 70% film (static contact angle 150.7 ± 0.4°) is slightly more hydrophobic than the 85% film (static contact angle 149.2 ± 0.6°). The influence of particle size and weight percentage on sliding angles is shown in Fig. 7 (b). The smallest sliding angles are reached on 70% FNP doped films in each group, and those with 85% FNP also have decent water repellent properties with sliding angles less than 10°. This is in accordance with our

observation that the water droplets are more prone to roll off surfaces with high percentage of nanoparticles. Superhydrophobicity is reached on the film with 70% 510 nm FNP, giving a static contact angle of 151.1 ± 0.3° and sliding angle of 5.5 ± 0.6°.

Ogihara et al. reported that the static contact angle reaches 148° on paper spray-coated with alkyl silane modified silica nanoparticles[26]. These authors suggest that nanometer- and micrometer-sized roughness was formed by the particles. As mentioned above, the presence of a hierarchical structure contributes favorably to superhydrophobicity. In their work, there is inherently roughness within paper structure itself, which is augmented by the spray coating. In the work presented here, smooth glass slides were used as substrates. The structural attributes of the surfaces arise solely from the silica particles, the polymer, and the method of application. The surface hydrophobicity is comparable to those on rough substrate, with static contact angles reaching as high as ~151°. We are able to modulate the wetting behavior of smooth surfaces by simply adjusting the composition of the coating solution. It has been reported that the wetting behavior of superhydrophobic coatings can be controlled by using particles of different sizes[50]. According to the cited work, the surface hydrophobicity increases with the particle size (40-300 nm) on all-particle coatings. In the current work, the surface hydrophobicity is easily tuned by adjusting the weight percentage of silica nanoparticles in the films, which is simple and effective. Brassard et al. also claimed that large particles provide more space for air entrapment, enhancing the water repellent performance according to the Cassie-Baxter model[50]. Interestingly, this is in contradiction with Saji et al. that larger silica particles (25, 250 and 500 nm were used in their experiments) showed less hydrophobicity on spray coated materials[69]. We find that the particle size is not as important as the particle wt%. However, in the 70% FNP-doped films the size dependence is in accordance with Brassard et al.'s statements: films doped with 120, 310 and

510 nm FNPs have static contact angles of 144.7 ± 0.8, 150.7 ± 0.2 and 151.1 ± 0.3 °, respectively. At other $wt\%_{FNP}$, however, this trend is not obeyed strictly. In the 30% FNP doped films, for instance, those with 120 nm FNPs (static contact angle 135.4 ± 0.4 °) are more hydrophobic than the 310 nm FNPs doped counterparts (static contact angle 130.3 ± 0.6 °). Both Brassard and Saji agreed that the volume of voids increase with particle size, but they reached opposite conclusions. Based on our observations, while particle size has an influence, it is by no means the most significant variable. The most significant variable is the particle wt%. An inference from the data is thus that the structures created, the random piles of particles arising from the three particle sizes, are probably on average geometrically similar. In this way, as the droplet contact area per particle increases, so does the area in contact with trapped air.

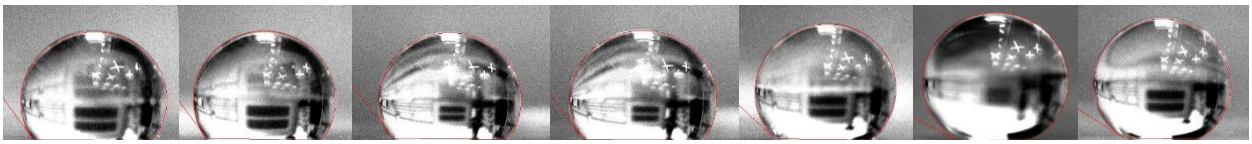

5% 10% 15% 30% 50% 70% 85%

Fig. 6 Static contact angle measurement on Teflon AF 2400 films with 5%, 10%, 15%, 30%, 50%, 70% and 85% (wt%) 510nm FNP.

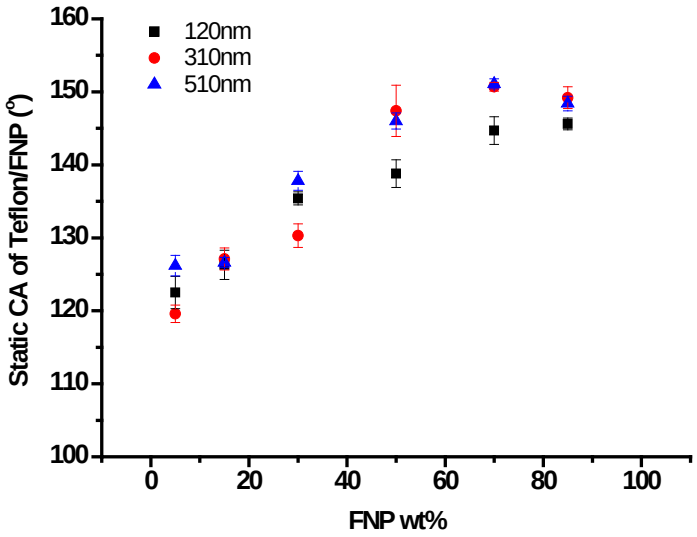

(a)

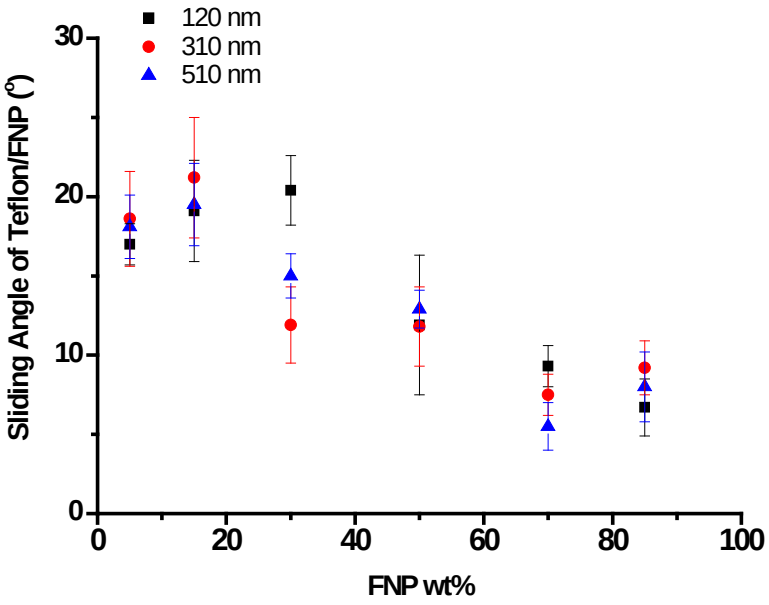

(b)

Fig. 7 Static contact angle (a) and sliding angle (b) of 4 μL water on spin-coated surfaces. Films were prepared with 120, 310 and 510nm FNPs, with wt% $_{FNP}$ of 5%, 10%, 15%, 30%, 50%, 70% and 85%.

3.3 SURFACE MORPHOLOGY ANALYSIS

AFM images were used to investigate the effect of surface morphology on film wettability. According to the 3D images of 70% FNP-doped Teflon films (Fig. 8), spherical particles piled up randomly in clusters, instead of forming mono- or multilayer arrays on the surface. The qualitative picture provided by the images is supported by quantitative estimates of roughness. The experimental RMS roughness was much larger than the calculated values based on the hexagonal close-packed monolayer (Table 1).

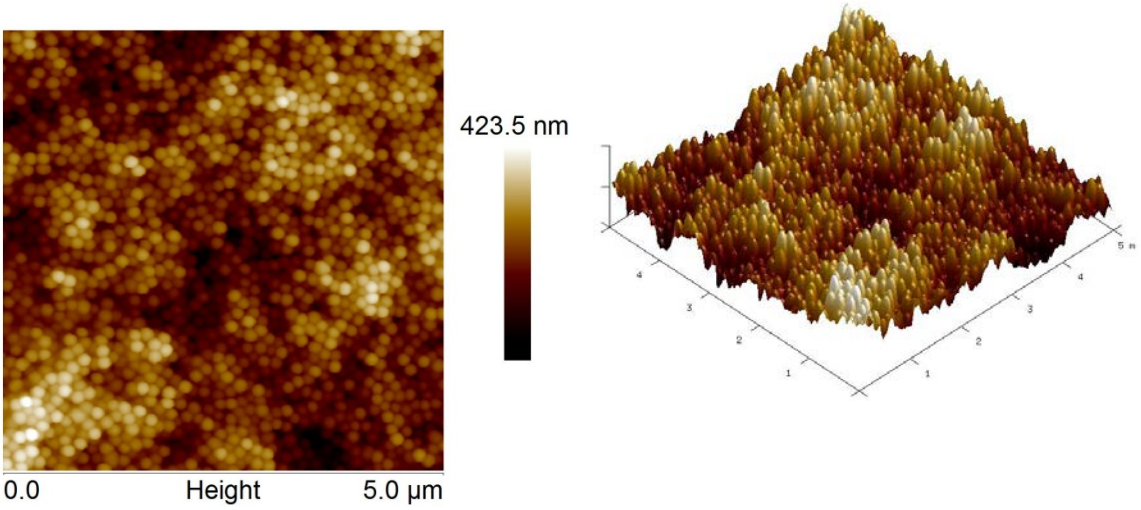

(a)

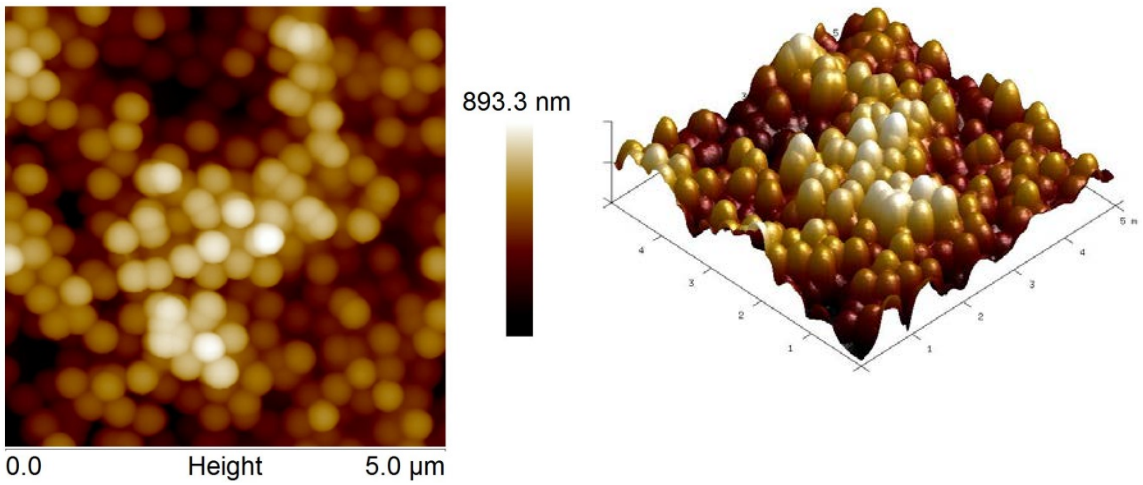

(b)

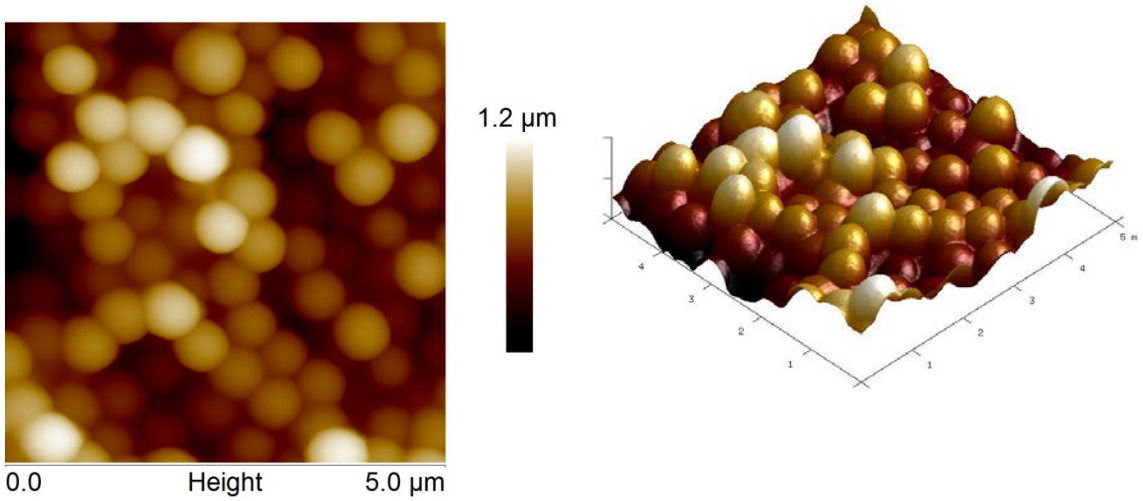

(c)

Fig. 8 AFM images of (a) 120nm, (b) 310nm, (c) 510nm FNP (wt% = 70%) doped Teflon films with 5µm scan size.

Table 1: Summary of wettability measurements and comparison to calculated values.

FNP	RMS (experimental, nm)*	RMS (theoretical, nm) ‡	*r* §	static contact angle (°)	Wenzel contact angle Θ_e^W (°)Ω	C-B contact angle Θ_e^{C-B} (°)Ω
120nm	60.8	14.8	1.436	144.7 ± 1.9	126.7	139.7
310nm	158	38.1	1.552	150.7 ± 0.6	130.2	141.3
510nm	199	62.7	1.480	151.1 ± 0.7	128.0	140.3

*RMS(experimental) = $[\Sigma(Z_i - Z_{ave})^2 / N]^{1/2}$, where Z_{ave} = Z value at the central plane, Z_i= local Z value, and N = number of points within the given area.

‡ RMS (theoretical) ≈ $0.123D$[70], based on close - packed model

§ *r*= Image Surface Area/ Image Projected Area

Ω Θ_e^W is the static contact angle predicted with Wenzel's model: $\cos\Theta_e^W = r\cos\Theta_o$, where the static contact angle on pure Teflon AF 2400 surface is Θ_o=114.6°; Θ_e^{C-B} is the static contact angle predicted with modified Cassie-Baxter's equation: $\cos\Theta^{C-B} = \Phi_B(\cos\Theta_o+1)^2-1$

As Table 1 shows, there was only a minor variance in static contact angle from 144.7± 0.1 to 151 ± 0.3° as the RMS roughness increased from 60.8 to 199nm, which is an indication that the degree of wetting was not affected significantly by surface scale length. This agrees with our and others'[71] statements that the wetting properties are not determined by particle size.

The surface roughness was also evaluated with the Wenzel roughness factor, *r*, which is the ratio of real surface area and the corresponding projected area. As the particle sizes increased from 120 to 510nm, the changes in *r* factors were quite small (1.436 to 1.552). According to Saito et. al, *r* is a constant in a hemispherical close-packed model and $r \approx 1.9$[72].The *r* value on surfaces with randomly packed particles must be larger than 1.9, consistent with its higher effective roughness. This indicates an underestimation of *r* values in our AFM measurement,

where $r \approx 1.4$~1.5. This is likely due to the fact that the AFM tip only probed the top of the particles and failed to insert into the narrow, deep cavities. Similar issues of roughness underestimation due to limitations of the AFM tips were seen by other groups recently[71,73].

As discussed previously, the hydrophobic states are described with two well-established models, where water can either fill up the rough surface or partially sits on it with air trapped below. As shown in Table 1, the measured static contact angles are larger than those predicted by Wenzel's model, with a discrepancy of more than 18°. This suggests that the Wenzel model is not adequate for description of the hydrophobic states on Teflon films, and the contribution from Cassie-Baxter's roughness, which creates the cavities between the particles trapped with air, should be considered. The static contact angle was estimated with a modified Cassie-Baxter's equation that $\cos\Theta^{C\text{-}B} = \Phi_B(\cos\Theta_o+1)^2-1$[74], where Φ_B is the ratio of the projected solid surface to the real surface area. As shown in Table 4, this equation is a closer prediction of the surface hydrophobic state than Wenzel, confirming that the Cassie-Baxter's model provides better description to surface roughness.

3.4 SOLUTION-CAST DEPOSITION

It is of interest to know the effect of the method of application. Thus, the hydrophobic performances of films prepared by spin-coating and solution-cast deposition are compared in Fig. 9 for particle diameter 120 nm. Even though there are only small differences in static contact angles between films with the same wt% $_{FNP}$, the sliding angles on spin-coated films are much smaller than those on cast films when wt% $_{FNP}$ > 30%. For instance, the static contact angles of spin-coated and cast films with 50% FNP are 138.8 ± 0.8 and 141.2 ± 0.2°, respectively; while

their sliding angles are 11.9 and 56°, respectively. Actually, the spin-coated and cast films have particles packed in roughly a similar manner, as can be told from the SEM images in Fig 10. A close investigation of the two images in Fig. 10, however, reveals that deep and wide grooves are formed in the spin-coated films, compared with the small and scattered cavities found in the cast ones. Moreover, FNPs in the cast films appear uniform in size and spherical (as they appear alone in the SEM image in Fig. 5). In spin-coated films, however, the particles appear different from those in Fig. 5. Many are not spherical, and they are not as monodisperse. We attribute this to the effect of the time scale difference in the two process on the polymer matrix that results. In the solvent cast films, polymer molecules have sufficient time to relax, approaching a minimum free energy. Evidence for this can be seen in the voids left by particles that have been dislodged (Fig. 10b). The voids are circular. In several cases, the circular edge of the cavities can be seen. This must be the polymer matrix. The thickness of these edges is quite uniform. The nonspherical shape of the particles in Fig. 10a, and the absence of obvious cavities imply that the polymer is coated onto individual particles at different thicknesses.

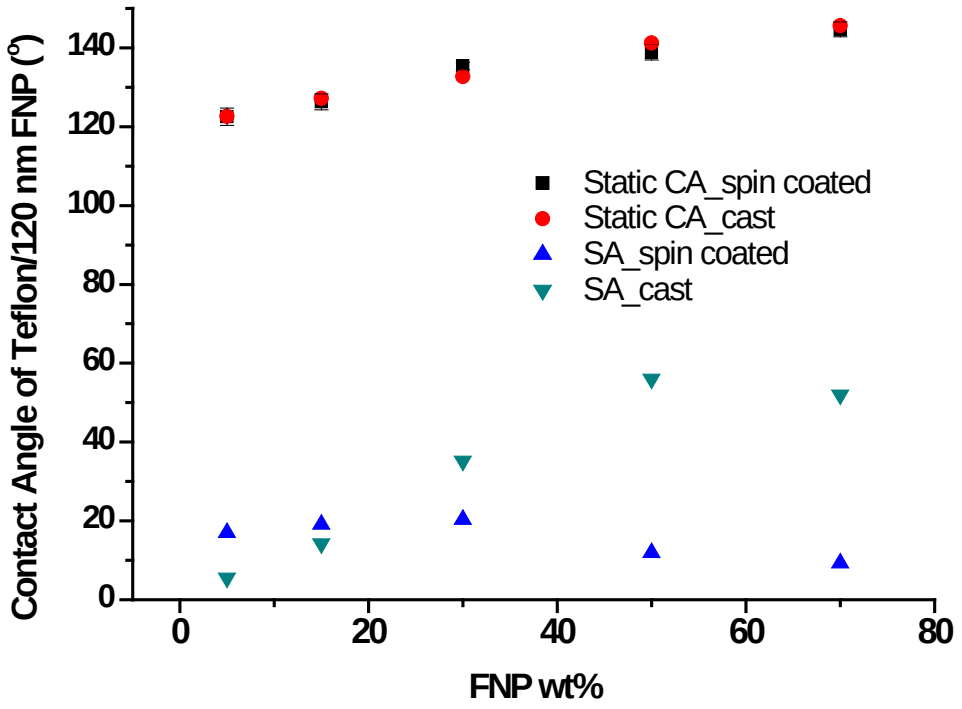

Fig. 9 The static contact angle and sliding angle of spin coated and solution-cast 120nm FNP doped Teflon films

Interestingly, the sliding angles of cast films increase with $wt\%_{FNP}$, following an opposite trend as in the spin-coated series. Specifically, the sliding angles increase from 5.5 to 56° as the $wt\%_{FNP}$ varies from 5% to 50%, while the static contact angles are steady at ~120 to 130°. The measurements are supported by our qualitative observations that even though water drops form spherical shapes on the cast films, they cannot slide well as the FNP percentage increases. A similar observation was made recently by Bayer et al. on sandpapers on which submicrometer Teflon particles had been deposited. They found that the sliding angle increased from ~10 ° to ~ 40 ° as the surface had more Teflon particles per unit area[65].

Obviously, solution-cast deposition (5-7 days) is much slower compared with spin coating (40 s for one layer). Therefore, FNPs have enough time to array and organize on the

substrate in solution-cast deposition. In spin-coating, however, the mobility of FNPs is prohibited because of the fast evaporation of solvent. In our case, the boiling point of the spin solvent is very low (b.p FC-72 = 56 °C, at 1 atm), which means its evaporation is much faster in the open air than in the half-sealed containers.

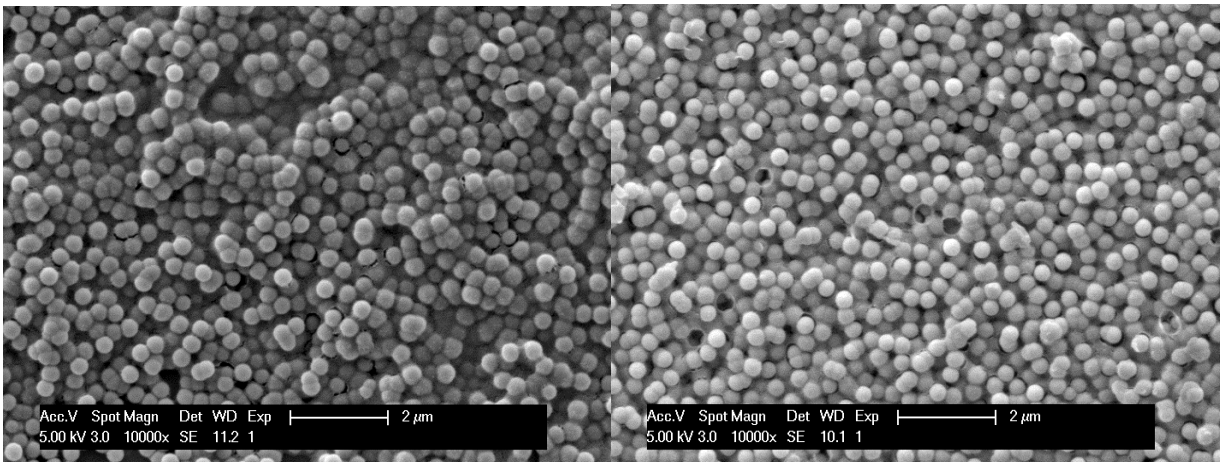

(a) (b)

Fig. 10 SEM images and of (a) spin-coat and (b) solution-cast deposited films with 70% (wt%) 120nm FNP.

4.0 CONCLUSION

We have demonstrated an easy and fast approach to prepare hydrophobic surfaces. For the first time, Teflon AF 2400 was spin-coated on glass slides with FNPs (diameter 120, 310 and 510 nm). The degree of wetting is a function of the weight percentage of particles. Specifically, we found that increasing the $wt\%_{FNP}$ from 5% to 70% benefits the surface structure in a way that the degree of wetting can be modulated with flexibility. The influence of particle size was found less significant than what was seen previously[50]. The random piles of particles of the three sizes are probably on average geometrically similar. Superhydrophobic states were achieved on spin-coated films with 70% weight percent 510 nm FNPs.

Teflon AF 2400 introduces low surface energy and increased surface durability in comparison to particle-only counterparts[46,50]. Moreover, the surface hydrophobicity on our Teflon AF films is solely attributable to the hierarchical roughness created by FNPs and the method of application. This approach does not depend on the underlying material structure[54-59]. Furthermore, we showed that spin-coated Teflon AF surfaces have smaller sliding angles than those fabricated by solution cast deposition, as a result of the restricted mobility of the FNPs in the spinning process. This work provides a simple approach to superhydrophobic painting with Teflon AF-containing FNP suspensions.

ACKNOWLEDGEMENT

We thank PPG Industries (PA), Glass Business and Discovery Center for help on the AFM.

BIBLIOGRAPHY

(1) Roach, P.; Shirtcliffe, N. J.; Newton, M. I. *Soft Matter* **2007**, *4*, 224.

(2) Lafuma, A.; Quere, D. *Nature materials* **2003**, *2*, 457.

(3) Ma, M.; Hill, R. M. *Current Opinion in Colloid & Interface Science* **2006**, *11*, 193.

(4) Neinhuis, C.; Barthlott, W. *Annals of Botany* **1997**, *79*, 667.

(5) Marmur, A. *Langmuir* **2004**, *20*, 3517.

(6) Cao, L.; Jones, A. K.; Sikka, V. K.; Wu, J.; Gao, D. *Langmuir* **2009**, *25*, 12444.

(7) Zhang, X.; Shi, F.; Niu, J.; Jiang, Y.; Wang, Z. *Journal of Materials Chemistry* **2008**, *18*, 621.

(8) Cassie, A.; Baxter, S. *Transactions of the Faraday Society* **1944**, *40*, 546.

(9) Yoshimitsu, Z.; Nakajima, A.; Watanabe, T.; Hashimoto, K. *Langmuir* **2002**, *18*, 5818.

(10) Ming, W.; Wu, D.; van Benthem, R.; With, G. d. *Nano Letters* **2005**, *5*, 2298.

(11) Zhai, L.; Cebeci, F. Ç.; Cohen, R. E.; Rubner, M. F. *Nano Letters* **2004**, *4*, 1349.

(12) Fürstner, R.; Barthlott, W.; Neinhuis, C.; Walzel, P. *Langmuir* **2005**, *21*, 956.

(13) Öner, D.; McCarthy, T. J. *Langmuir* **2000**, *16*, 7777.

(14) Zhang, Y.; Lo, C.-W.; Taylor, J. A.; Yang, S. *Langmuir* **2006**, *22*, 8595.

(15) Nosonovsky, M.; Bhushan, B. *Nano Letters* **2007**, *7*, 2633.

(16) Ming, W.; Wu, D.; van Benthem, R.; de With, G. *Nano Letters* **2005**, *5*, 2298.

(17) Qian, Z.; Zhang, Z.; Song, L.; Liu, H. *Journal of Materials Chemistry* **2009**, *19*, 1297.

(18) Leng, B.; Shao, Z.; de With, G.; Ming, W. *Langmuir* **2009**, *25*, 2456.

(19) Lin, P.-C.; Yang, S. *Soft Matter* **2009**, *5*, 1011.

(20) Stöber, W.; Fink, A.; Bohn, E. *Journal of colloid and interface science* **1968**, *26*, 62.

(21) Hench, L. L.; West, J. K. *Chemical Reviews* **1990**, *90*, 33.

(22) Green, D.; Lin, J.; Lam, Y. F.; Hu, M. Z. C.; Schaefer, D. W.; Harris, M. *Journal of colloid and interface science* **2003**, *266*, 346.

(23) Tsai, H.-J.; Lee, Y.-L. *Langmuir* **2007**, *23*, 12687.

(24) Karunakaran, R. G.; Lu, C. H.; Zhang, Z.; Yang, S. *Langmuir* **2011**, *27*, 4594.

(25) Ling, X. Y.; Phang, I. Y.; Vancso, G. J.; Huskens, J.; Reinhoudt, D. N. *Langmuir* **2009**, *25*, 3260.

(26) Ogihara, H.; Xie, J.; Saji, T. *Colloids and Surfaces A: Physicochemical and Engineering Aspects* **2013**.

(27) Wallqvist, V.; Claesson, P. M.; Swerin, A.; Östlund, C.; Schoelkopf, J.; Gane, P. A. C. *Langmuir* **2009**, *25*, 9197.

(28) Wenzel, R. N. *Ind. Eng. Chem* **1936**, *28*, 988.

(29) Wang, B.; Zhang, Y.; Shi, L.; Li, J.; Guo, Z. *Journal of Materials Chemistry* **2012**.

(30) Quéré, D. *Nature materials* **2002**, *1*, 14.

(31) Bico, J.; Thiele, U.; Quéré, D. *Colloids and Surfaces A: Physicochemical and Engineering Aspects* **2002**, *206*, 41.

(32) Gladysz, J. A.; Curran, D. P.; Horvath, I. T. *Handbook of fluorous chemistry*; Wiley-VCH, 2006.

(33) Hildebrand, J. H.; Scott, R. L. **1955**.

(34) Goss, K.-U.; Bronner, G. *The Journal of Physical Chemistry A* **2006**, *110*, 9518.

(35) O'Neal, K. L.; Zhang, H.; Yang, Y.; Hong, L.; Lu, D.; Weber, S. G. *Journal of Chromatography A* **2010**, *1217*, 2287.

(36) Kiss, L. E.; Kövesdi, I.; Rábai, J. *Journal of fluorine chemistry* **2001**, *108*, 95.

(37) Studer, A.; Hadida, S.; Ferritto, R.; Kim, S. Y.; Jeger, P.; Wipf, P.; Curran, D. P. *Science* **1997**, *275*, 823.

(38) Luo, Z.; Zhang, Q.; Oderaotoshi, Y.; Curran, D. P. *Science* **2001**, *291*, 1766.

(39) Curran, D.; Lee, Z. *Green Chemistry* **2001**, *3*, G3.

(40) Curran, D. P. *Pure and Applied Chemistry* **2000**, *72*, 1649.

(41) Curran, D. P.; Oderaotoshi, Y. *Tetrahedron* **2001**, *57*, 5243.

(42) Chhatre, S. S.; Guardado, J. O.; Moore, B. M.; Haddad, T. S.; Mabry, J. M.; McKinley, G. H.; Cohen, R. E. *Fluoroalkylated silicon-containing surfaces-Estimation of solid surface energy*, DTIC Document, 2010.

(43) Zhou, H.; Wang, H.; Niu, H.; Gestos, A.; Wang, X.; Lin, T. *Advanced Materials* **2012**.

(44) Saleema, N.; Sarkar, D.; Gallant, D.; Paynter, R.; Chen, X. G. *ACS Applied Materials & Interfaces* **2011**, *3*, 4775.

(45) Campos, R.; Guenthner, A. J.; Haddad, T. S.; Mabry, J. M. *Langmuir* **2011**, *27*, 10206.

(46) Brassard, J. D.; Sarkar, D.; Perron, J. *Applied Sciences* **2012**, *2*, 453.

(47) Jisr, R. M.; Rmaile, H. H.; Schlenoff, J. B. *Angewandte Chemie International Edition* **2005**, *44*, 782.

(48) Akram Raza, M.; Kooij, E. S.; van Silfhout, A.; Poelsema, B. *Langmuir* **2010**, *26*, 12962.

(49) Lau, K. K. S.; Bico, J.; Teo, K. B. K.; Chhowalla, M.; Amaratunga, G. A. J.; Milne, W. I.; McKinley, G. H.; Gleason, K. K. *Nano Letters* **2003**, *3*, 1701.

(50) Brassard, J. D.; Sarkar, D.; Perron, J. *ACS Applied Materials & Interfaces* **2011**, *3*, 3583.

(51) Nilsson, M. A.; Daniello, R. J.; Rothstein, J. P. *Journal of Physics D: Applied Physics* **2010**, *43*, 045301.

(52) Singh, E.; Chen, Z.; Houshmand, F.; Ren, W.; Peles, Y.; Cheng, H. M.; Koratkar, N. *Small* **2013**, *9*, 75.

(53) Zhang, H.; Hussam, A.; Weber, S. G. *Journal of the American Chemical Society* **2010**, *132*, 17867.

(54) Kannarpady, G. K.; Khedir, K. R.; Ishihara, H.; Woo, J.; Oshin, O. D.; Trigwell, S.; Ryerson, C.; Biris, A. S. *ACS Appl. Mater. Interfaces* **2011**, *3*, 2332.

(55) Thieme, M.; Blank, C.; Pereira, d. O. A.; Worch, H.; Frenzel, R.; Hoehne, S.; Simon, F.; Lewis, H. G. P.; White, A. J. *Contact Angle, Wettability Adhes.* **2009**, *6*, 251.

(56) Wu, J.; Xia, J.; Lei, W.; Wang, B.-p. *Mater. Lett.* **2010**, *65*, 477.

(57) An, T.; Cho, S. J.; Choi, W.; Kim, J. H.; Lim, S. T.; Lim, G. *Soft Matter* **2011**, *7*, 9867.

(58) Kolomytkin, D. O.; Gallyamov, M. O.; Khokhlov, A. R. *Russ. J. Phys. Chem. B* **2011**, *5*, 1106.

(59) Lifton, V. A.; Simon, S. *J. Porous Mater.* **2011**, *18*, 535.

(60) Han, D.; Steckl, A. J. *Langmuir* **2009**, *25*, 9454.

(61) Muthiah, P.; Hsu, S.-H.; Sigmund, W. *Langmuir* **2010**, *26*, 12483.

(62) Scheffler, R.; Bell, N. S.; Sigmund, W. *J. Mater. Res.* **2010**, *25*, 1595.

(63) Liu, Y.; Chen, X.; Xin, J. H. *Nanotechnology* **2006**, *17*, 3259.

(64) Liu, Y.; Chen, X.; Xin, J. H. *J. Mater. Chem.* **2009**, *19*, 5602.

(65) Bayer, I. S.; Brandi, F.; Cingolani, R.; Athanassiou, A. *Colloid and Polymer Science* **2013**, *291*, 367.

(66) Chang, J. F.; Sun, B.; Breiby, D. W.; Nielsen, M. M.; Sölling, T. I.; Giles, M.; McCulloch, I.; Sirringhaus, H. *Chemistry of materials* **2004**, *16*, 4772.

(67) Bao, Z.; Dodabalapur, A.; Lovinger, A. J. *Applied Physics Letters* **1996**, *69*, 4108.

(68) Wang, G.; Swensen, J.; Moses, D.; Heeger, A. J. *Journal of applied physics* **2003**, *93*, 6137.

(69) Ogihara, H.; Xie, J.; Okagaki, J.; Saji, T. *Langmuir* **2012**, *28*, 4605.

(70) Oudrhiri-Hassani, F.; Presmanes, L.; Barnabé, A.; Tailhades, P. *Applied Surface Science* **2008**, *254*, 5796.

(71) Hansson, P. M.; Skedung, L.; Claesson, P. M.; Swerin, A.; Schoelkopf, J.; Gane, P. A. C.; Rutland, M. W.; Thormann, E. *Langmuir* **2011**, *27*, 8153.

(72) Nakae, H.; Inui, R.; Hirata, Y.; Saito, H. *Acta materialia* **1998**, *46*, 2313.

(73) Fritzen-Garcia, M. B.; Zanetti-Ramos, B. G.; de Oliveira, C. S.; Soldi, V.; Pasa, A. A.; Creczynski-Pasa, T. B. *Materials Science and Engineering: C* **2009**, *29*, 405.

(74) Bico, J.; Marzolin, C.; Quéré, D. *EPL (Europhysics Letters)* **1999**, *47*, 220.